Determination of the moisture diffusivity of rammed earth from transient capillary absorption moisture content profiles

Margaux Indekeu, Hans Janssen, Monika Woloszyn

Version of Record: https://www.sciencedirect.com/science/article/pii/S0950061821037107
Manuscript_f4a0059f0ee3379c836a4c7e095b2fc8

Determination of the moisture diffusivity of rammed earth from transient capillary absorption moisture content profiles

Margaux L. Indekeu [a,*], Hans Janssen [b], Monika Woloszyn [a]

[a] Université Savoie Mont Blanc, CNRS, LOCIE, 73000 Chambéry, France

[b] KU Leuven, Department of Civil Engineering, Building Physics and Sustainable Design, 3001 Leuven, Belgium

* Corresponding author. E-mail address: margaux.indekeu@live.be.

Graphical abstract

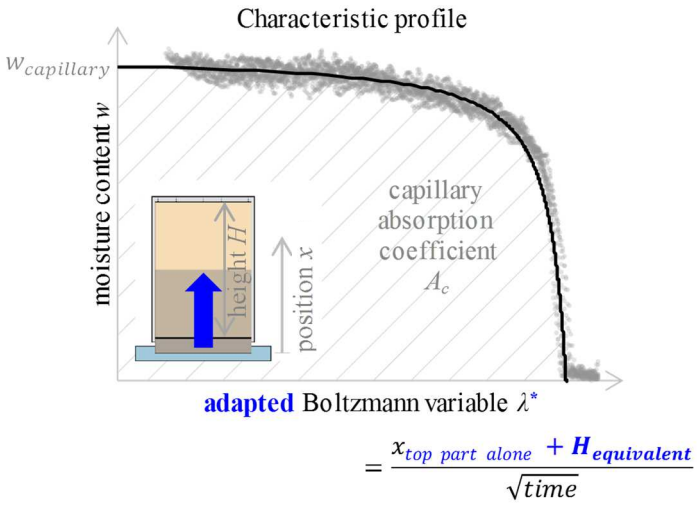

Abstract

The determination of the moisture diffusivity in the capillary range is studied for rammed earth building materials, using the X-ray method. To prevent liquefaction and expansion of these materials during the capillary absorption test, a brick wick and paper are added as lower sample parts and a confining sealing is utilised. Since the wick and paper bring about a composite case, the compatibility with the Boltzmann transformation must be redeveloped. It is found that the solution lies in adjusting the Boltzmann transformation through the equivalent height capturing the hydraulic impact of the wick and paper on the capillary absorption process.

Keywords

rammed earth; moisture diffusivity; capillary absorption; X-ray radiography; moisture profile; multilayer composite; Boltzmann transformation; equivalent length; characteristic profile

Highlights

- The moisture diffusivity of rammed earth is studied by modifying the X-ray method.
- A confinement eliminates disturbances by material evolution during the test.
- The Boltzmann transformation is corrected for the presence of a wick and paper.

- This is done via their hydraulically equivalent height in the capillary absorption.
- Taking this equivalent height into account is indispensable for the studied cases.

1 Introduction

Historical rammed earth buildings are widely present in several countries, including European countries such as France and Spain [1]. To gain insight via numerical simulation (in contrast to hygrothermal monitoring [2-4]) into their hygrothermal behaviour and the possibilities to (thermally) retrofit these constructions, the hygric (and thermal) material properties are needed as input. Owing to the inherent difficulties to measure their moisture behaviour, however, there is a lack of knowledge on the moisture transfer properties of rammed earth materials, particularly in the over-hygroscopic range (> 97% relative humidity) [5-8]. These over-hygroscopic properties nonetheless need to be determined as well, since rammed earth building walls under atmospheric excitation in practice are also exposed to driving rain, rising damp, …

The moisture retention curve and the moisture permeability curve are typically required as input in simulations. The moisture retention curve is presumed to be available in the present study. The moisture permeability curve can be determined as the product of the moisture diffusivity function and the moisture capacity function, the derivative of the moisture retention curve. The moisture diffusivity is typically determined through analysis of moisture content profiles monitored during moisture transfer experiments. Visualisation of the profiles with X-ray radiographic measurements during capillary absorption testing is commonly used for this, to deliver the moisture diffusivity in the high range [9-12].

For rammed earth materials, the capillary absorption test has been adapted to avoid material evolution, particularly liquefaction and expansion [13,14]. Specifically, a thin permeable brick wick and contact paper (at the interface) are introduced as lower sample parts to counter the liquefaction, and a confining sealing is applied to counter the expansion [14]. Because the wick and paper are inherently initially dry in the confined setup, they offer an hydraulic resistance and the protocol becomes an absorption in a multilayer composite [14-17] rather than in a single material. This implies that the capillary absorption behaviour of the target top material is only retrieved after a certain interval. The determination of the moisture diffusivity from the moisture content profiles relies on the Boltzmann transformation [9-12], which however requires that the sample is suitably homogenous and exhibits the ideal [18] square root of time moisture absorption behaviour right from the start. For the determination of the moisture diffusivity, these lower parts hence induce a complication regarding the compatibility with the Boltzmann transformation method.

The target of this paper is hence to redevelop the Boltzmann transformation method to enable its proper application to composite cases as involved for the determination of the liquid water diffusivity of rammed earth building materials. The associated research question is: ‘How to adapt the Boltzmann transformation method in the advanced capillary absorption test methodology for the multi-layer composite case involving the wick and paper for rammed earth materials, to determine their moisture diffusivity?’.

In Section 2, first, information on the materials used is provided. The pore volume distribution and the basic hygric properties of the rammed earth materials studied, as well as of the brick wick material, are collected. Subsequently, the measurement set-up, the experimental procedure, and the data acquisition of the composite capillary absorption test with X-ray radiography are presented. In Section 3, the theoretical background founding

the experimental determination of the moisture diffusivity is reiterated. From there, the physical foundations of the Boltzmann transformation method for composite cases are developed. The correct performance of the modified determination method is subsequently validated experimentally using a sample of a stable material that is investigated both with and without lower parts. The fitting method for the characteristic Boltzmann transformed profile is thereafter explained. In Section 4, the results of the modified determination method are presented for the rammed earth materials. The modified method's robustness for the rammed earth cases is finally demonstrated by illustrating the influence of not correcting the Boltzmann transformation for the presence of the wick and paper.

2 Materials and experiment

2.1 Material information

Two rammed earth target materials are extracted from traditional rammed earth buildings in the Auvergne-Rhône-Alpes region, France [14]. Both materials are relatively homogenous (they have an insignificant gravel fraction). For the rammed earth material of house 1 (H1), it is known that it contains 15% sand, 65% silt, and 20% clay fraction [19], and that the clay fraction comprises illite and vermiculite [20]. This information is not available for the H6 rammed earth material. The H1 rammed earth is, for operational reasons, crushed [21] and reconstructed in the lab via ramming by a craftsman [14]. For the H6 rammed earth, cohesive samples are used directly, extracted via core drilling [14]. Fig. 1 shows the pore volume distribution (f_v, kg/(m³log$_{10}$(Pa))) for wetting of these materials against the logarithmic capillary pressure (p_c, Pa), determined by means of a combination of mercury intrusion porosimetry and desiccator testing (and capillary absorption testing for the upper limit), and Table 1 collects their basic hygric properties [14]. All properties are defined relative to the 70°C oven dry state. The volume for the bulk density is determined as part of the mercury intrusion porosimetry test procedure, the open porosity is determined through the mercury intrusion porosimetry in combination with the desiccator testing, and the moisture content at 75% relative humidity (RH) is determined by means of desiccator testing.

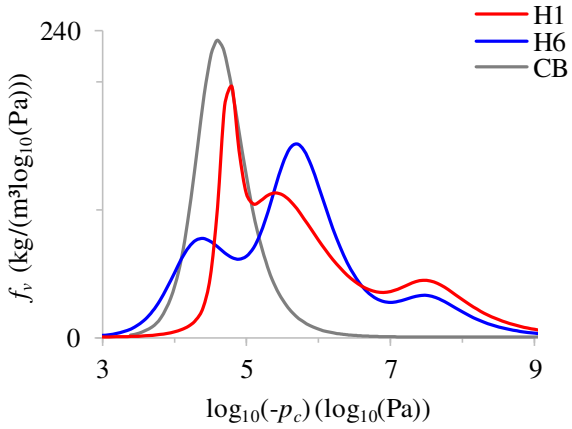

Fig. 1: Pore volume distribution (wetting) versus capillary pressure of rammed earth materials H1 and H6, as well as of ceramic brick wick material. The curve fittings are adjusted relative to in Indekeu et al. [14] according to recent findings and insights.

Table 1: Basic hygric properties of rammed earth materials H1 and H6, as well as of ceramic brick wick material, with material error (%).

	Bulk density (kg/m^3)	Open porosity (m^3/m^3)	Moisture content at 75% RH (kg/m^3)	Capillary absorption coefficient ($kg/(m^2s^{0.5})$)[a]	Capillary moisture content (kg/m^3)
H1	1757 (±1.9%)	0.352 (±5.6%)	35.0 (±0.6%)	0.262 (±5.7%)	288 (±1.5%)[b]
H6	1708 (±2.7%)	0.338 (±2.4%)	18.4 (±20.3%)	0.188 (±18.1%)	296 (±3.2%)
CB[c]	1818 (±0.9%)	0.326 (±4.1%)	< 1.0 (±13.5%)	0.61 (±15.2%)	210 (±4.3%)

[a] At 22.6 °C on average.

[b] Deviation instead of standard deviation because only two results are involved.

[c] Taken from Feng et al. [18;22].

The capillary absorption properties of the rammed earth materials in Table 1 result from confined composite testing [14]. Four samples per rammed earth material are involved. In Indekeu et al. [14], it is shown that if the sample is not confined, these absorption properties undesirably increase by ca. 39% for the capillary absorption coefficient and by 31% for the capillary moisture content for the H1 rammed earth, e.g (the H6 rammed earth expands less). The materials have an ideal capillary absorption behaviour.

To minimise the delay in obtaining the target capillary absorption behaviour in the composite test, it is of interest that the material of the thin wick (preferably as thin (short) as possible) has a larger liquid permeability than the target materials (and preferably as large as possible). A ceramic brick (CB) material is hence used as wick; its pore volume distribution and basic hygric properties are included in Fig. 1 and Table 1, respectively. In addition, the contact paper (filter/blotting, cf. Table 2) at the interface offers also already an hydraulic resistance [14] (besides that it enhances the hydraulic contact through its fibres).

2.2 Test setup, procedure, and data acquisition

The measurement set-up of the capillary absorption experiment with X-ray radiography with a composite sample, Fig. 2 (a), is shown in Fig. 2 (b). Table 2 gives an overview of the samples used in the present study. Two duplicate samples are tested for each of the two rammed earth materials. The sample thickness and X-ray energy (see below) are chosen appropriately for an optimal moisture content resolution [10], given that the water attenuation coefficient values for rammed earth (ca. 20.76 m^{-1} (average 20 pixels width and full width, cf. below), obtained from the results) are similar as for ceramic brick [24]. The samples are despite their small thickness considered representative of the rammed earth due to the low gravel content [14]. The 1 cm high wick is half-immersed. The wick and the fibrous paper contact layer counter the liquefaction of the rammed earth material. The rammed earth sample is confined with (first cling film to avoid epoxy penetration and then) epoxy resin at the lateral and top sides and is attached to the wick at the bottom side, to avoid expansion and keep it mechanically stable [14]. This confinement also facilitates accurately determining the moisture content at each position and the attachment to the wick moreover enhances the hydraulic contact. The whole assembly is initially

dry because of this attachment (that is realised prior to the testing). That is why absorption in a composite applies. The sample is positioned between the X-ray source and detector, at a distance of ca. 107 cm from the source and as close as possible to the detector (21 x 21 cm², see Fig. 2 (b)). The source is set for 80 kV energy during each scan (the current is 215 µA and the iris position is 85.0). Dummies are included in the set-up as a reference for calibration [23] to compensate for the instability of the X-ray source over time. These are small dry samples of different materials (metal, ceramic brick, tile, and calcium silicate) that give attenuated intensities in a range that (largely) covers the target sample (including its moisture content). The linear calibration curve is also forced to go through the origin (i.e. the source is off). The water is deionised, 23.2 µS/cm electrical conductivity, and 1 °C below the 24.7 °C (average) temperature in the X-ray chamber.

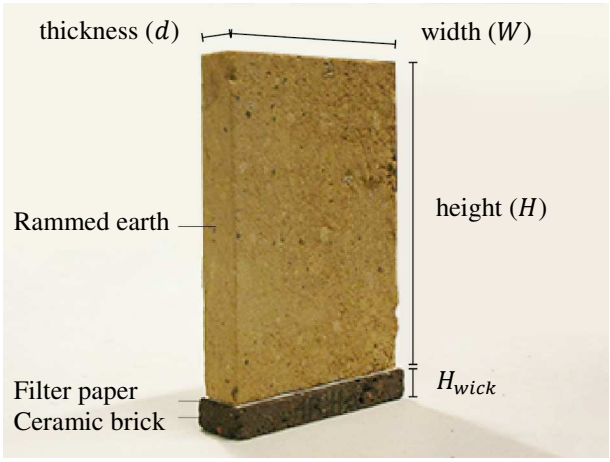

(a)

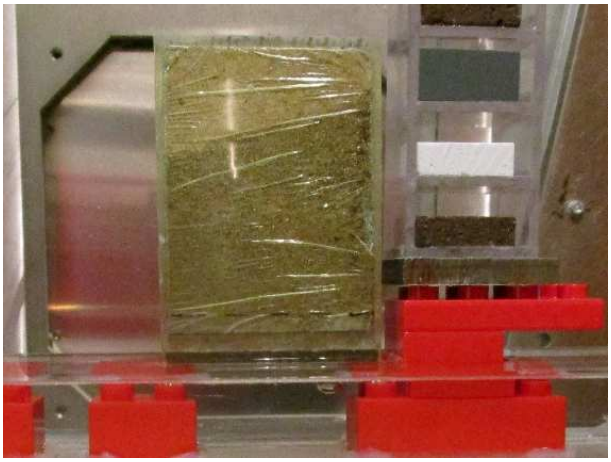

(b)

Fig. 2: (a) Composite sample of ceramic brick wick, filter paper and H1 rammed earth material; (b) Set-up of capillary absorption test with X-ray radiography.

Table 2: Overview of confined composite rammed earth samples for capillary absorption test with X-ray radiography. The ceramic brick sample used for the validation in Section 3.2 is included as well.

Rammed earth material	H1		H6		CB
	Sample 1	Sample 2	Sample 1	Sample 2	
H (cm)	9.3	9.2	6.2	6.0	12.1
W (cm)	6.6	6.4	6.4	6.4	8.0

d (cm)	1.4	1.4	1.5	1.4	2.0
H_{wick} (cm)	1.0	1.0	1.0	1.0	- or 1.0
paper type	blotting	filter	filter	filter	- or blotting

The experimental procedure consists of measuring the moisture distribution during the capillary absorption regularly in time by means of X-ray projection. Tomohawk equipment is used for this as well as a Matlab code to read the intensity values in the resulting radiation files. For one image, 256 projections are averaged, resulting in a time resolution of 22 s. The first, dry reference image is taken as soon as possible after the water touches the assembly (this usually comes down to at ca. 37 s). The test should preferably be continued sufficiently long to enable determining the capillary moisture content. Immediately after the final wet image, the sample is weighed. This will enable determining the effective water attenuation coefficient [24] (through Eq. (1)). The moisture mass of the wick that is subtracted for this, is estimated as the average of its vacuum saturation and its capillary moisture content (the paper's moisture mass is neglected).

In the data processing, the moisture content (w, kg/m³) at each position in the rammed earth part in time is quantified by logarithmically subtracting the reference image of the dry sample from the images of the wetting sample Eq. (1) [10]. The symbols herein further stand for the density of water (ρ_{wat}, kg/m³), the effective water attenuation coefficient (μ_{wat}, m^{-1}), the sample thickness (d, m), and the wet/dry transmitted intensity ($I_{wet/dry}$, -). The estimated real edges [10] are used as the rammed earth sample borders in the image.

$$w = -\frac{\rho_{wat}}{\mu_{wat} d} \ln\left(\frac{I_{wet}}{I_{dry}}\right) \tag{1}$$

For the determination of the moisture content profiles, only the data in a column in the middle of the sample are used to avoid distortions. This column is taken 20 pixels wide for averaging to reduce the scatter [10]. This corresponds to ca. 2.7 mm width for the studied cases. For the composite test analysis, the capillary absorption process plot of the sample needs to be determined in addition to the moisture content profiles. This is necessary to determine the equivalent height of the lower parts for the Boltzmann transformation, see Sections 3 and 4. It is obtained from the moisture distributions measured, using the full sample width for representativeness in determining the accumulated moisture (in the top part alone). In Indekeu et al. [14], it is shown that the capillary absorption process plotted based on the X-ray data in this way closely matches that obtained from a lab test with the same sample, whereby the former is shown to be reliable.

3 Theoretical background and methodology

3.1 Modified Boltzmann approach

The theoretical background for the experimental determination of the moisture diffusivity [9-11] follows from the one-dimensional isothermal moisture mass conservation equation Eq. (2). Darcy's law is used for the transport term. Formulated with the moisture diffusivity (D_m, m²/s), describing the moisture transport using the moisture content (w, kg/m³) as the driving potential instead of moisture permeability (k_m, s) with gradients of capillary pressure (p_c, Pa), this becomes a partial differential equation with the moisture content as a function of the time (t, s) and the position (x, m) in the transport direction:

$$\frac{\partial w}{\partial t} = -\frac{\partial}{\partial x}\left(-k_m \frac{\partial p_c}{\partial x}\right) = -\frac{\partial}{\partial x}\left(-\frac{k_m}{\frac{\partial w}{\partial p_c}}\frac{\partial w}{\partial x}\right) = -\frac{\partial}{\partial x}\left(-D_m \frac{\partial w}{\partial x}\right) \quad (2)$$

The equation can, by substituting the Boltzmann variable (λ, m/s$^{0.5}$) Eq. (3), be reduced to an ordinary differential equation Eq. (4). The associated initial (w_{ini}) Eq. (5) and boundary (w_{bou}) Eqs. (6) and (7) Boltzmann conditions state that the porous medium is initially at a uniform moisture content, subsequently exposed to a constant boundary condition at one surface, and can be regarded as semi-infinite, respectively.

$$\lambda = \frac{x}{\sqrt{t}} \quad (3)$$

$$\frac{-\lambda}{2}\frac{dw}{d\lambda} = -\frac{d}{d\lambda}\left(-D_m \frac{dw}{d\lambda}\right) \quad (4)$$

$t = 0$ (and $x > 0$) → $\lambda \to \infty$: $w = w_{ini}$ (5)

$t > 0$ and $x = 0$ → $\lambda = 0$: $w = w_{bou}$ (6)

$t > 0$ and $x \to \infty$ → $\lambda \to \infty$: $w = w_{ini}$ (7)

Provided that the porous medium can be considered homogenous and that the investigated resulting moisture transfer process in it behaves linearly with the square root of time, the Boltzmann transformed transient moisture content profiles - scaled to the square root of time - collapse to form the characteristic w-λ profile. Integration of Eq. (4) leads to the unique solution of the moisture diffusivity as a function of the moisture content Eq. (8). Hence it appears that the moisture diffusivity can be obtained by integrating and differentiating the characteristic profile as a function of the moisture content. The boundary moisture content for capillary absorption tests is assumed to be equal to the capillary moisture content. The integral under the characteristic profile is equal to the capillary absorption coefficient.

$$D_m(w) = \frac{-\frac{1}{2}\int_{w_{ini}}^{w} \lambda \, dw}{\left.\frac{dw}{d\lambda}\right|_w} \quad (8)$$

In several studies [14,15,17], it is shown that in the case of a composite sample, from the moment that the persistent linear capillary absorption pattern of the top material is retrieved, the target sample behaves as if it were preceded by a certain length of its own material: the hydraulically equivalent height (see Appendix for its exact definition). This equivalent height (H_{equ}, m) is hence used to correct the Boltzmann transformation as in Eq. (9). The remaining symbols herein stand for the adapted Boltzmann variable (λ^*, m/s$^{0.5}$) and the position in the top part alone (x_{tpa}, m). This equation can also be derived theoretically based on a simplified sharp front model, see Appendix. The equivalent height corresponds to the fitted intercept of the accumulated moisture in the top (i.e. rammed earth) part alone (m_{tpa}, kg/m²) against the square root of time [14]: Fig. 3, Eqs. (10) and (11). The coefficient of determination (R^2, -) that remains greater than 0.999 collecting data points from the end of the persistent linear first stage backward in time, is used as the criterion to determine this exact fitting firmly. The symbols herein further stand for the capillary absorption coefficient (A_c, kg/(m^{2}s$^{0.5}$)) of the top material (C for the tri-layer composite of application [14]), the equivalent accumulated moisture (m_{equ}, kg/m^2), and the

capillary moisture content (w_{cap}, kg/m^3) of the top material.

$$\lambda^* = \frac{x_{tpa} + H_{equ}}{\sqrt{t}} \tag{9}$$

$$m_{tpa} = A_{c,C}\sqrt{t} - m_{equ} \tag{10}$$

$$H_{equ} = \frac{m_{equ}}{w_{cap,C}} \tag{11}$$

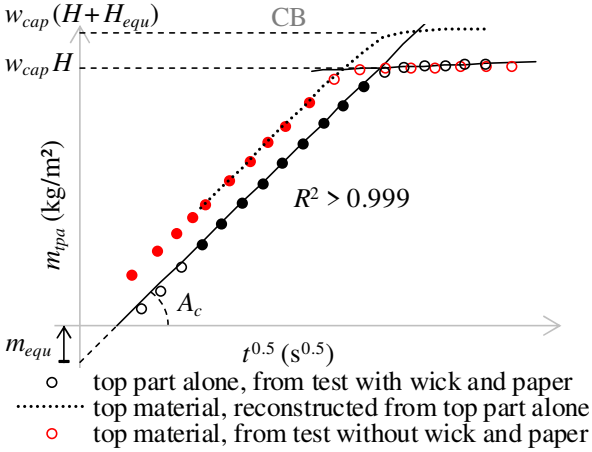

Fig. 3: Demonstration of data processing methodology using ceramic brick example – part I. Capillary absorption process from test with or without wick and paper (Section 3.2). Filled markers indicate data used for fitting, supported by coefficient of determination. Hydraulic impact of lower parts is translated into equivalent height of target material.

As a function of the adapted Boltzmann variable, the transformed moisture content profiles should collapse without systematic time tendency to form the characteristic profile, Eqs. (12) to (15). The yet undefined symbols herein stand for the actual (t_B, s) and the equivalent time at which the moisture front reaches the second junction (t_{equ}, s) of the tri-material composite, and the height ($H_{A/B}$, m) of material A/B. Integration of Eq. (12) leads to the expression for the calculation of the target moisture diffusivity as a function of the moisture content, Eq. (16). The characteristic profile is connected to the capillary moisture content at the (equivalent) boundary, cf. Fig. 4. It should be identical to the characteristic profile for the single material case and the surface area under it should be equal to the capillary absorption coefficient, Eq. (17).

$$\frac{-\lambda^*}{2}\frac{dw}{d\lambda^*} = -\frac{d}{d\lambda^*}\left(-D_{m,C}\frac{dw}{d\lambda^*}\right) \tag{12}$$

$$t + t_{equ} - t_B\ (\approx t) = 0 \text{ (and } x - H_A - H_B + H_{equ} > 0) \rightarrow \lambda^* \rightarrow \infty\text{: } w = w_{ini,C} \tag{13}$$

$$t + t_{equ} - t_B\ (\approx t)\ > 0 \text{ and } x - H_A - H_B + H_{equ} = 0 \rightarrow \lambda^* = 0\text{: } w = w_{bou,C} \tag{14}$$

$$t + t_{equ} - t_B\ (\approx t) > 0 \text{ and } x - H_A - H_B + H_{equ} \rightarrow \infty \rightarrow \lambda^* \rightarrow \infty\text{: } w = w_{ini,C} \tag{15}$$

$$D_{m,C}(w) = \frac{-\frac{1}{2}\int_{w_{ini,C}}^{w} \lambda^* \, dw}{\frac{dw}{d\lambda^*}\Big|_w} \tag{16}$$

$$A_{c,C} = \int_{w_{ini,C}}^{w_{bou,C}} \lambda^* \, dw = \int_{0}^{w_{cap,C}} \lambda^* \, dw \tag{17}$$

3.2 Validation of approach

The correct performance of the physically/theoretically redeveloped Boltzmann approach for composite cases is validated experimentally. A sample of a stable, ceramic brick, material is used for this, to enable comparison of the result of a test without and with lower parts (wick & paper). The sample dimensions and composing parts are given in Table 2. Specifically, the objective is to verify to which extent the characteristic profile from a standard test with the standard Boltzmann transformation and the characteristic profile from a composite test with the adapted Boltzmann transformation, coincide. Fig. 4 shows the results (the corresponding capillary absorption process plots are given in Fig. 3; the equivalent height amounts to 1.66 cm). It is observed that the resulting characteristic profiles/scatter bands agree as one. So the validation was successful. The increased degree of scatter for the composite can be linked to the swelling of the blotting paper during wetting, since the ceramic brick sample is not confined. The surface area under the characteristic profile equals the capillary absorption coefficient.

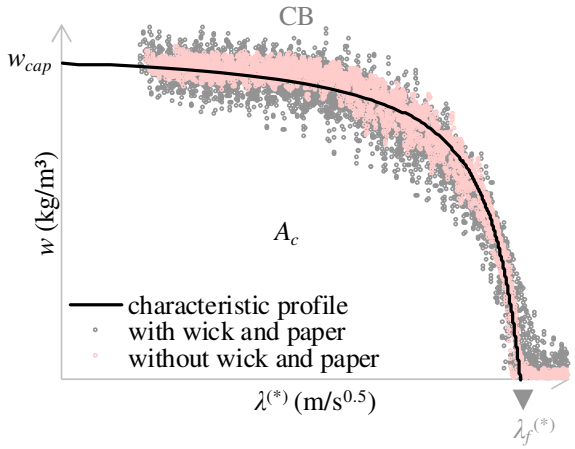

Fig. 4: Demonstration of data processing methodology using ceramic brick example – part II. Characteristic profile and Boltzmann transformed moisture content profile data from test with (λ^*) or without (λ) wick and paper.

Fig. 5 shows for comparison the error when the Boltzmann transformation is not corrected for the composite case (λ^-, m/s$^{0.5}$), i.e. x_{tpa} is used without adding H_{equ} in the numerator Eq. (9). It is observed that the capillary absorption coefficient is underestimated by ca. 17% (the profiles do not collapse as well). This deviation is unacceptable since it is greater than ceramic brick repeatability (±2.1%) [22], or even material (see Table 1), errors.

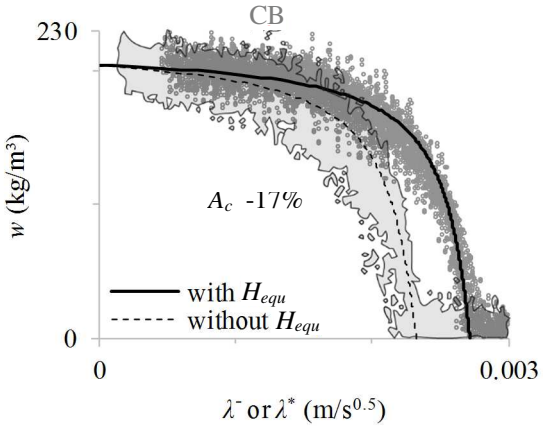

Fig. 5: Demonstration of data processing methodology using ceramic brick example – part III. Characteristic profile and scatter band with (λ^*) or without (λ^-) taking into account equivalent height in Boltzmann transformation.

3.3 Characteristic profile fitting

The smooth characteristic profile fitting, based on which the moisture diffusivity is determined (cf. Eqs. (8) and (16)), should fall within the random scatter band. Various possibilities exist to fit the characteristic profile [25-27]. The tangent formula [12,27] is used in the present work: Eq. (18) with boundary conditions Eqs. (19) and (20) and with the requirement that the surface area under the characteristic profile is fitted correctly. The yet undefined symbols herein are the fitting parameters a, b and c and the average boundary lambda value (λ_f, m/s$^{0.5}$), see Fig. 4. The motive for preferring this fitting method in the present work is its straightforwardness, as well as its apparently reasonable suitability, see Section 4.1. It is particularly convenient for bridging the data-less zone that corresponds to the equivalent preceding sample part from the adapted Boltzmann transformation.

$$\lambda^{(*)}(w) = \frac{1}{b}\left(\tan\left(-\frac{w + w_{cap}}{a}\right) - c\right) \tag{18}$$

$$w = w_{cap} : \lambda^{(*)} = 0 \tag{19}$$

$$w = 0 : \lambda^{(*)} = \lambda_f^{(*)} \tag{20}$$

4 Results and discussion

4.1 Results of modified determination method

The results of the modified determination method for the rammed earth materials are presented. Fig. 6 shows the capillary absorption process (a) for the H1 samples and (b) for the H6 samples. The inset summarises the resulting properties. For all samples, a persistent linear first stage pattern is retrieved, which indicates that it is dominated by the rammed earth material properties [14]. The aberrant process course for the H1 sample 2 can be explained by the slight hourglass shape of the sample, see Fig. 2 (b). The resulting equivalent heights are always

positive, which affirmatively indicates that the lower parts (wick & paper) offer an hydraulic resistance. The equivalent heights for the H6 samples are typically larger than for H1, in spite of the smaller capillary absorption coefficient (in combination with the similar capillary moisture content). This indicates most probably an influence of the hydraulic contact quality through sample roughness [14]. The equivalent height magnitudes vary considerably for the duplicate samples of both materials, which can be explained by the reasons mentioned above, and/or by the material heterogeneity for H6.

Only the H6 sample 2 test is continued sufficiently long to determine the capillary moisture content. The other tests are for operational reasons already stopped just after the moisture front reaches the sample top. The average (avg) capillary moisture content of the material (for sample 1 of H1 and H6) from Table 1 or the final (w_{fin}) moisture content measured if this is greater than the average capillary moisture content (for H1's sample 2) is hence used instead for these other samples (for the determination of the equivalent height and as the boundary moisture content of the characteristic profile, e.g.). The impact of this should remain limited as there is only little variation in the capillary moisture content between different samples (see Table 1).

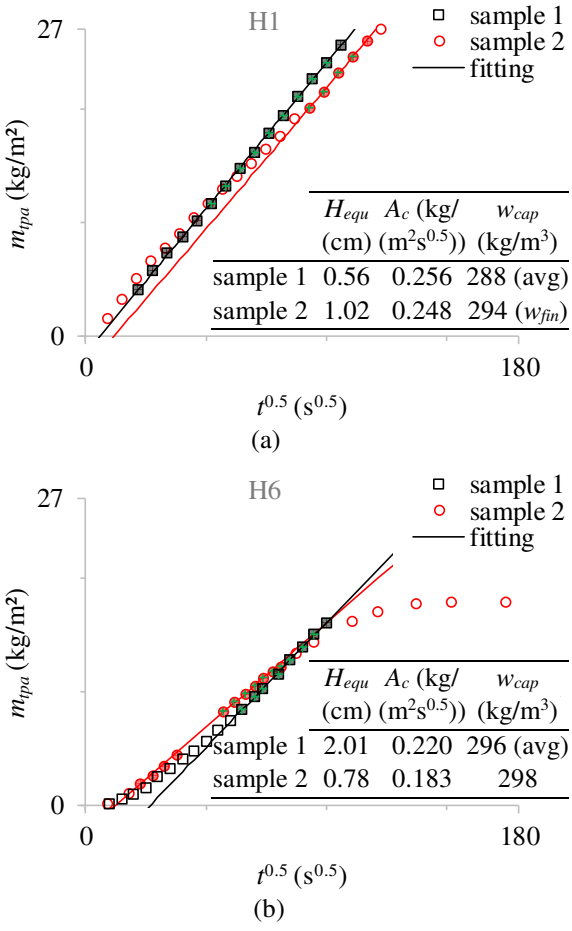

Fig. 6: Capillary absorption process with accumulated moisture in top (i.e. rammed earth) part alone (a) for H1 samples and (b) for H6 samples. Markers of data selected for fitting supported by coefficient of determination (> 0.999) are filled. Crossed markers furthermore indicate data of profiles kept after Boltzmann transformation.

Fig. 7 illustratively shows the moisture content profiles (a) for the H1 sample 1 and (b) for the H6 sample 1. It is observed that a sharp front is formed and the capillary moisture content is approached at the

boundary. A larger equivalent height yields a smaller moisture content at the boundary. The data in the erroneous zone at the boundary wherein the calculated moisture contents are incorrect, possibly caused by the timing of the reference image and/or by spatial [10] conflicts, are further discarded. For the determination of the capillary absorption process (Fig. 6), these values are pragmatically replaced by a linear connection to the average rammed earth material capillary moisture content from lab tests [14] at the boundary. The profile line types distinguish the profiles that obey the linearity rule and the profiles that are moreover retained after the Boltzmann transformation because they form the characteristic band. These latter are also cross-marked in Fig. 6. The profiles that do not satisfy the Boltzmann conditions (linearity & semi-infinity), i.e. the 'unselected profiles' and the final profiles, are further discarded.

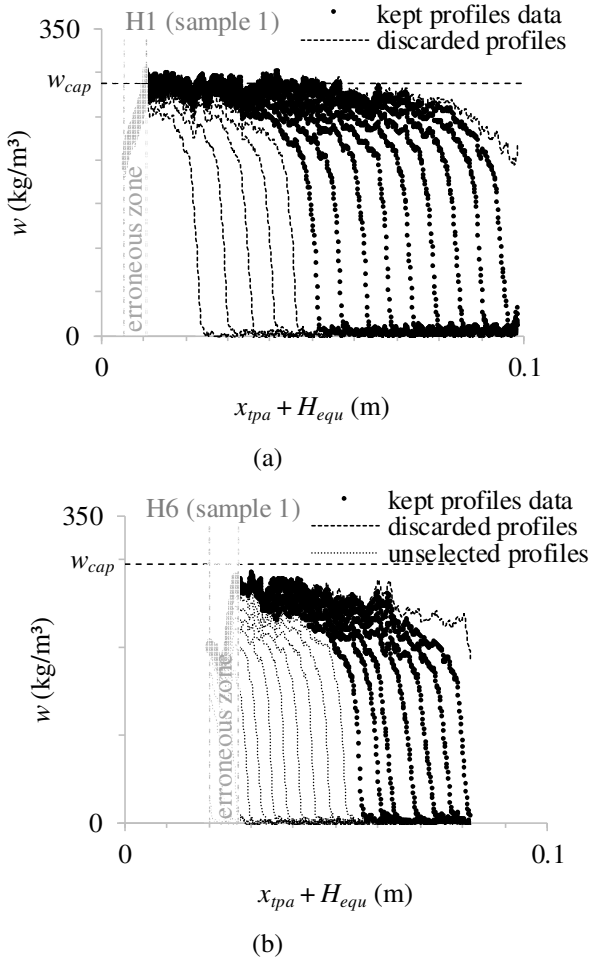

Fig. 7: Transient capillary absorption moisture content profiles in top part alone versus total (equivalent) height (a) for H1 sample 1 and (b) for H6 sample 1. Time steps are given in Fig. 6.

Fig. 8 shows the Boltzmann transformed moisture content profiles and the characteristic profile fitting (a) for the H1 rammed earth samples and (b) for the H6 rammed earth samples. It is observed that (most of) the transformed profiles successfully collapse (except a few early profiles for the H1 sample 1 and for the H6 sample 2, that are further discarded). The surface area under the characteristic profile equals the capillary absorption coefficient (from Fig. 6). The redeveloped Boltzmann transformation thus performs correctly. The characteristic

profile fitted with the tangent formula falls overall approximately in the middle of the scatter band (for H1 somewhat more than for H6). It is hence considered sufficiently accurate.

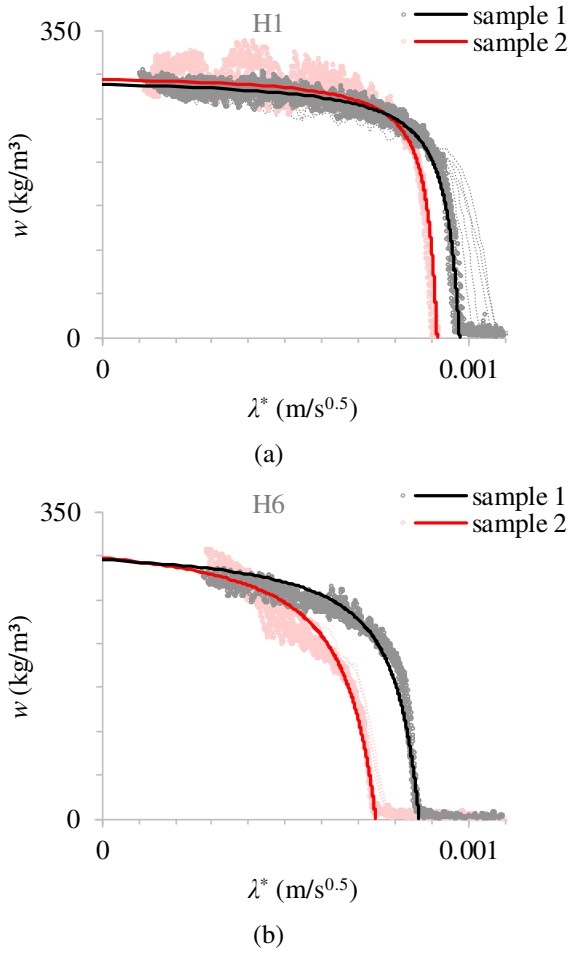

Fig. 8: Characteristic profile fitting and underlying Boltzmann transformed moisture content profiles (a) for H1 rammed earth samples and (b) for H6 rammed earth samples. Discarded profiles are indicated with dashed line.

Fig. 9 shows the moisture diffusivity (a) for the H1 rammed earth samples and (b) for the H6 rammed earth samples. It is observed that the apparently significant differences in the characteristic profiles of the duplicate samples (Fig. 8) still result in similar diffusivities (cf. Ren et al. [12]). So, the characteristic profiles are well-made.

The differences in diffusivity between the two materials are relatively more significant, Fig. 10. The moisture diffusivity of the H1 rammed earth is larger in the high range, that is relevant for the capillary transfer. This can be linked to its 'fuller' (more rectangular) characteristic profile shape.

It is verified that the determined diffusivity reproduces the capillary absorption behaviour (per sample) via numerical hygrothermal simulation. Delphin software [28] is used for this, which is based on the control volume method. A rammed earth sample of height $H + H_{equ}$ is simulated one-dimensionally, with the grid element size being 1 mm. The diffusivity is used directly as material (liquid water diffusivity) input [29] together with the moisture retention curve fitted to the capillary moisture content of the sample. A capillary pressure of 0 Pa is assigned to the sample bottom surface for water contact. The resulting simulated characteristic profile (not

shown) fits the experimental (Fig. 8) and the surface area under it equals the capillary absorption coefficient. To be precise, this is exact for the H6 samples, while for the H1 samples the simulation slightly (+2.0%) overestimates the capillary absorption coefficient in practice.

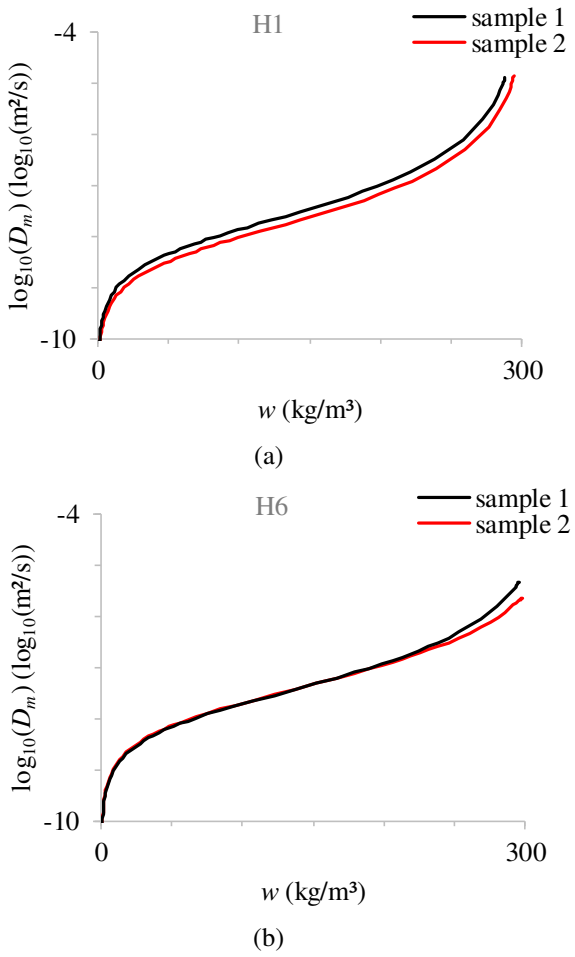

Fig. 9: Moisture diffusivity of target materials (a) H1 and (b) H6.

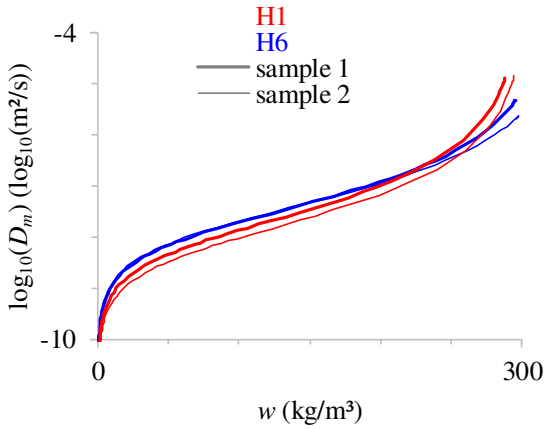

Fig. 10: Moisture diffusivity of target materials H1 and H6.

Fig. 11 shows the moisture permeability (a) for the H1 rammed earth samples and (b) for the H6 rammed earth samples. The moisture permeability is determined as the product of the moisture diffusivity and the moisture capacity, see Eq. (2). The limited accuracy in determining the moisture capacity when nearing capillary saturation yields an unphysically decreasing permeability in that range. It is therefore corrected enforcing a constant permeability [9]. The numerical simulation is performed again with the permeability as input this time to verify that the same behaviour is still reproduced. If necessary, the upper limit of the permeability is slightly adjusted (lowered, in practice) to fit this reproduction. The resulting permeabilities, shown in Fig. 11, are similar for the duplicate samples.

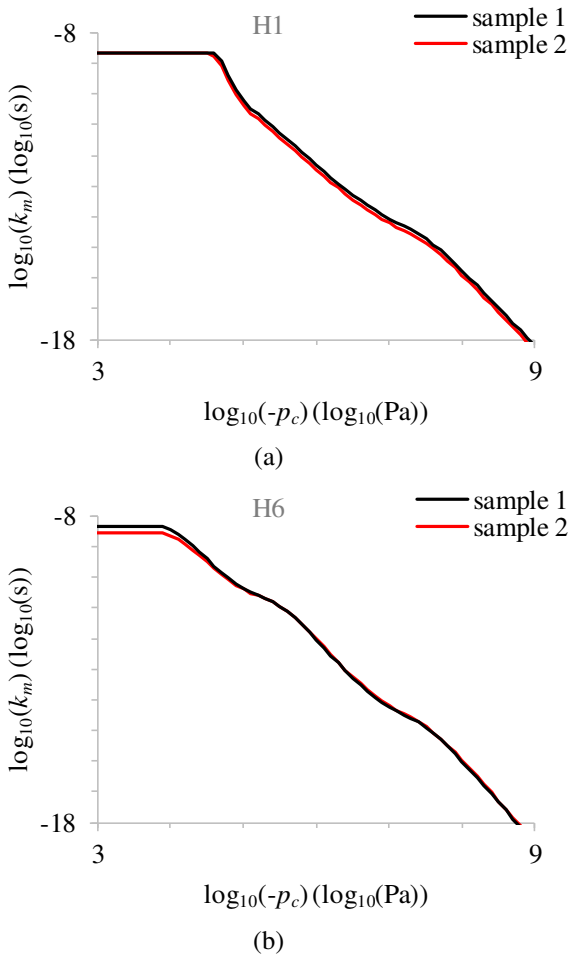

Fig. 11: Moisture permeability of target materials (a) H1 and (b) H6.

Fig. 12 shows the average moisture permeability for the H1 rammed earth and for the H6 rammed earth. The shape of the permeability curve can be linked to the pore volume distribution, Fig. 1 (or moisture retention curve). The characteristic profile from a simulation with the average moisture permeability and the average moisture retention curve of the material works out in between the characteristic profiles of the duplicate samples. The target characterisation (up to the moisture permeability) is hereby successfully completed.

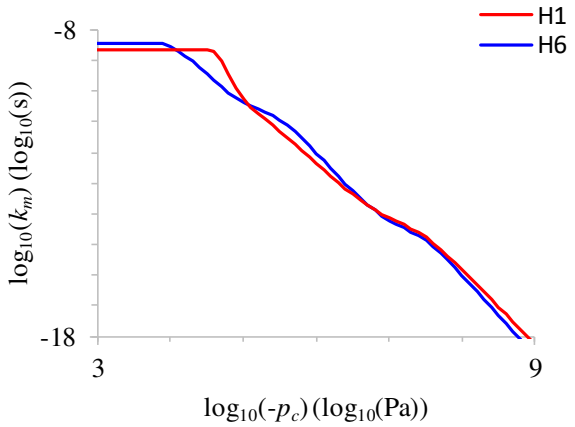

Fig. 12: Moisture permeability of target materials H1 and H6.

4.2 Impact of adapted Boltzmann variable

The impact of not taking into account the equivalent height in the Boltzmann transformation is demonstrated to assess the robustness of the modified determination method for the rammed earth cases (cf. Figs. 4 and 5 for the ceramic brick example). Fig. 13 shows the impact on the characteristic profile and hence the capillary absorption coefficient (a) for the H1 samples and (b) for the H6 samples, and Fig. 14 shows the impact on the average moisture permeability. It is observed that the permeability is systematically underestimated, and significantly (especially for H6). The reduction in the capillary absorption coefficient is larger than the deviation between the samples measured. This indicates an unacceptable procedural error that could lead to erroneous moisture estimations in a wall. The error increases with increasing equivalent height (and with decreasing capillary absorption coefficient). Fig. 15 illustratively shows the impact on the simulation of moisture content profiles (using the average properties) (a) for the H1 rammed earth and (b) for the H6 rammed earth. It is hence affirmatively concluded that for the investigated cases, it is necessary to take into account the equivalent height in the Boltzmann transformation for a reliable characterisation.

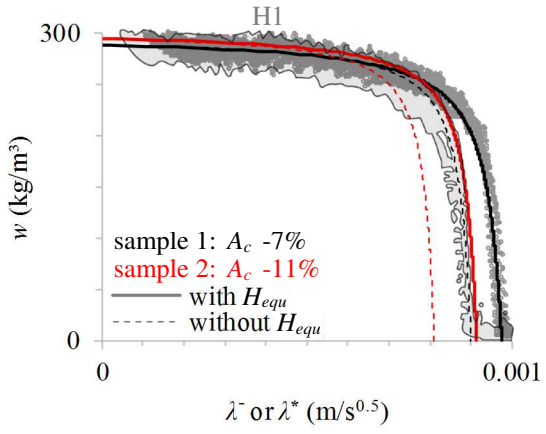

(a)

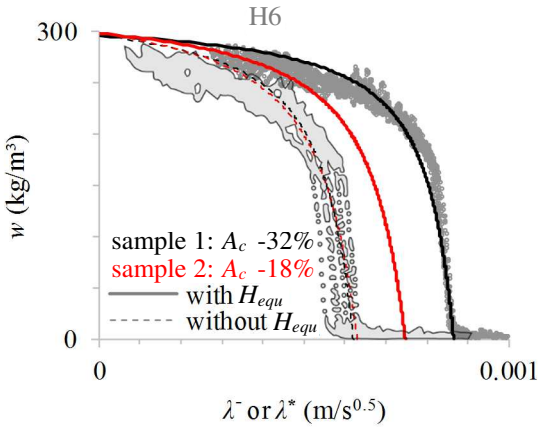

(b)

Fig. 13: Characteristic profile with (λ^*) or without (λ^-) taking into account equivalent height (a) for H1 samples and (b) for H6 samples. The associated scatter band is each time included for sample 1 only.

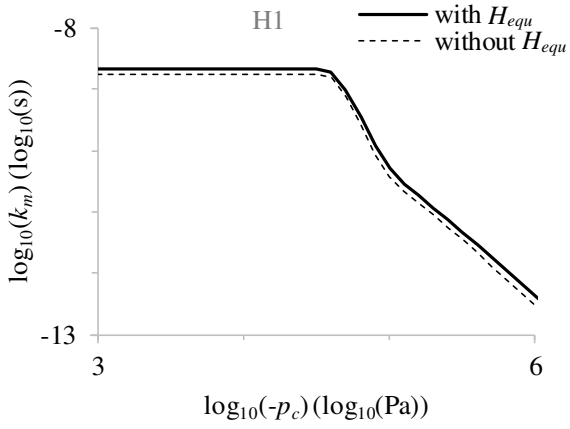

(a)

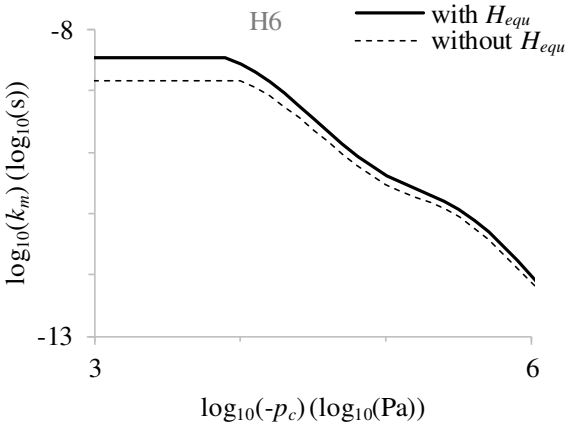

(b)

Fig. 14: Moisture permeability from characteristic profiles with or without taking into account equivalent height (a) for H1 rammed earth and (b) for H6 rammed earth. Only the high range, determinative for the capillary transfer, is shown.

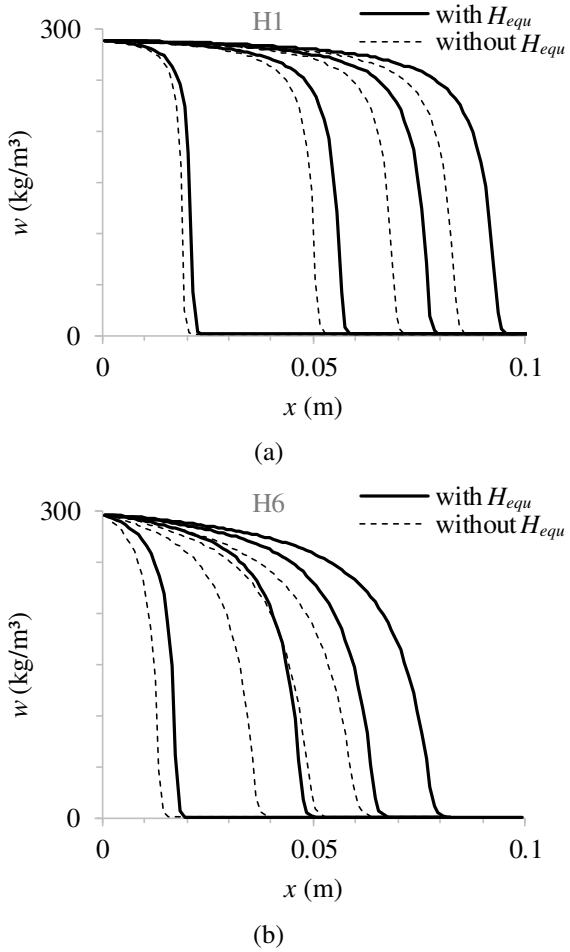

Fig. 15: Moisture content profiles at 500 s, 3500 s, 6500 s, and 9500 s, with or without taking into account equivalent height in Boltzmann transformation for characterisation (a) for H1 rammed earth and (b) for H6 rammed earth.

5 Conclusion

The moisture diffusivity in the over-hygroscopic range is determined for two different traditional rammed earth building materials with an insignificant gravel fraction. The well-established X-ray attenuation method is used for this (on thin prismatic samples), and it is adapted to be applicable for rammed earth, as following. The initially dry relatively short brick wick and contact paper assembled that avoid the rammed earth material liquefaction during the confined - to avoid the expansion - capillary absorption test bring about a composite situation. The Boltzmann transformation is made compatible with this by taking into account the hydraulically equivalent height of these lower parts in terms of the top material: $\lambda^* = \left(x_{tpa} + H_{equ}\right)/\sqrt{t}$. This equivalent height is determined based on the capillary absorption process of the sample, that is additionally deducted from the X-ray measurements (besides the moisture content profiles in time; in the rammed earth part alone). Resultantly, the intended characteristic profile is formed. The smaller the equivalent height, the more completely the characteristic profile, and hence the moisture diffusivity, is exactly determinable. The lower parts (wick & paper) should be as thin and permeable as possible for this. It is finally explicitly demonstrated that for the investigated cases, it is crucial to take into account the equivalent height (0.6 – 2 cm) in the Boltzmann

transformation, as this guarantees that the integral behaviour in time of the capillary absorption test is reproduced by the determined moisture diffusivity.

Acknowledgements

The research work presented is realised in the context of the first author's doctoral thesis (in progress) at the Université Savoie Mont Blanc and financed by the Région Auvergne-Rhône-Alpes. Much of the experimental activities have been performed in the facilities of KU Leuven, as a visiting scholar. The authors would like to acknowledge prof. dr. Chi Feng, dr. ir. Evy Vereecken, dr. Jeroen Soete, and ir. Johan Vanhulst for their practical advice with respect to experimental matters.

Appendix A. Theoretical substantiation of adapted Boltzmann variable

The Boltzmann transformation is founded on the square root of time moisture absorption behaviour. This behaviour can be demonstrated theoretically based on a sharp front model [18]. For the single material case, this leads to Eq. (A.1) for the penetration of the moisture front in the material. Rearranging gives a simplified equivalent of the definition of the Boltzmann variable (λ, m/s$^{0.5}$) Eq. (A.2). The water penetration coefficient (B, m/s$^{0.5}$) can thus be seen as the Boltzmann variable specifically at the critical moisture front position (x_{front}, m). The other symbols stand for the average moisture permeability in the wet zone ($k_{m,wet}$, s) of the sharp front model, the capillary pressure (p_c, Pa) at the sample surface in contact with water ($p_{c,0}$) or at the height of the moisture front position ($p_{c,cri}$), the time (t, s), the capillary moisture content (w_{cap}, kg/m^3), and the position (x, m).

$$x_{front} = \sqrt{\frac{2k_{m,wet}(p_{c,0} - p_{c,cri})t}{w_{cap}}} = B\sqrt{t} \tag{A.1}$$

$$\lambda = \frac{x}{\sqrt{t}} \tag{A.2}$$

For the tri-layer composite case with materials A, B, and C (wick, paper, and rammed earth), analogously, Eq. (A.3) can be derived for the penetration of the moisture front in the assembly [14]. From there, the definition of the adapted Boltzmann variable for composite cases (λ^*, m/s$^{0.5}$) is found, Eq. (A.4). The same equation can be derived based on a bi-layer case. The remaining symbols stand for the height (H, m) of materials, the equivalent height (H_{equ}, m) for the trilayer case and for the bilayer case ($H_{equ,bi}$), the capillary absorption coefficient (A_c, kg/(m^{2}s$^{0.5}$)), the actual (t_B) and the equivalent time (t_{equ}, s) at which the moisture front reaches the second junction, and the position in the top part alone (x_{tpa}, m).

$$x_{front} =$$

$$\sqrt{\frac{2k_{m,wet,C}\left(p_{c,0}-p_{c,cri,C}\right)}{w_{cap,C}}}$$

$$\cdot\sqrt{t+\frac{\left(k_{m,wet,C}\left(\frac{H_A}{k_{m,wet,A}}+\frac{H_B}{k_{m,wet,B}}\right)\right)^2 w_{cap,C}}{2k_{m,wet,C}\left(p_{c,0}-p_{c,cri,C}\right)}-\frac{\left({H_B}^2+2H_B\frac{k_{m,wet,B}}{k_{m,wet,A}}H_A\right)w_{cap,B}}{2k_{m,wet,B}\left(p_{c,0}-p_{c,cri,B}\right)}-\frac{{H_A}^2 w_{cap,A}}{2k_{m,wet,A}\left(p_{c,0}-p_{c,cri,A}\right)}}$$

$$-k_{m,wet,C}\left(\frac{H_A}{k_{m,wet,A}}+\frac{H_B}{k_{m,wet,B}}\right)+H_A+H_B \tag{A.3}$$

$$= B_C\sqrt{t+\frac{{H_{equ}}^2 w_{cap,C}}{2k_{m,wet,C}\left(p_{c,0}-p_{c,cri,C}\right)}-\frac{\left({H_B}^2+2H_B H_{equ,bi}\right)w_{cap,B}}{2k_{m,wet,B}\left(p_{c,0}-p_{c,cri,B}\right)}-\frac{{H_A}^2 w_{cap,A}}{2k_{m,wet,A}\left(p_{c,0}-p_{c,cri,A}\right)}}-H_{equ}+H_A$$

$$+H_B$$

$$= B_C\sqrt{t+\frac{{H_{equ}}^2 {w_{cap,C}}^2}{{A_{c,C}}^2}-t_B}-H_{equ}+H_A+H_B$$

$$= B_C\sqrt{t+t_{equ}-t_B}-H_{equ}+H_A+H_B$$

$$\overset{(for\ t\gg t_{equ}-t_B)}{\approx} B_C\sqrt{t}-H_{equ}+H_A+H_B$$

$$\lambda^* = \frac{x_{tpa}+H_{equ}}{\sqrt{t}} \tag{A.4}$$

Nomenclature

symbol	meaning	unit
a	fitting parameter	kg/m^3
A_c	capillary absorption coefficient	kg/(m^{2}s$^{0.5}$)
b	fitting parameter	s$^{0.5}$/m
B	water penetration coefficient	m/s$^{0.5}$
c	fitting parameter	-
d	thickness	m
D_m	moisture diffusivity	m^2/s
f_v	pore volume distribution	kg/(m^{3}log$_{10}$(Pa))
H	height	m
I	transmitted intensity	-
k_m	moisture permeability	s
m	accumulated moisture	kg/m^2
p_c	capillary pressure	Pa
R^2	coefficient of determination	-
t	time	s
w	moisture content	kg/m^3
W	width	m
x	position	m
λ	Boltzmann variable	m/s$^{0.5}$
λ^*	adapted Boltzmann variable	m/s$^{0.5}$
λ^-	adapted Boltzmann variable without taking into account equivalent height	m/s$^{0.5}$
λ_f	average boundary lambda value	m/s$^{0.5}$

μ_{wat}	effective water attenuation coefficient	m^{-1}
ρ_{wat}	density of water	kg/m^3
$_A$	of material A, i.e. the first, bottom, material of a composite sample	
$_B$	of material B, i.e. the second material of a composite sample	
$_{bi}$	bilayer	
$_{bou}$	boundary	
$_C$	of material C, i.e. the third material of a composite sample	
$_{cap}$	capillary	
$_{cri}$	critical	
$_{equ}$	equivalent	
$_{fin}$	final	
$_{ini}$	initial	
$_{tpa}$	top part alone	
$_0$	at 0 m position, i.e. at the water contact	
avg	average	
CB	ceramic brick	
H	house	
RH	relative humidity	

References

1] L. Fontaine, R. Anger, Bâtir en terre : du grain de sable à l'architecture, Belin, Cité des sciences et de l'industrie, Paris, 2009. https://craterre.hypotheses.org/451 (accessed 7 October 2021).

2] L. Soudani, M. Woloszyn, A. Fabbri, J.-C. Morel, A.-C. Grillet, Energy evaluation of rammed earth walls using long term in-situ measurements, Sol. Energy 141 (2017) 70–80. https://doi.org/10.1016/j.solener.2016.11.002.

3] D. Allinson, M. Hall, Hygrothermal analysis of a stabilised rammed earth test building in the UK, Energy Build. 42 (2010) 845–852. https://doi.org/10.1016/j.enbuild.2009.12.005.

4] E. Vereecken, S. Roels, A comparison of the hygric performance of interior insulation systems : A hot box–cold box experiment, Energy Build. 80 (2014) 37–44. https://doi.org/10.1016/j.enbuild.2014.04.033.

5] P. Gerard, M. Mahdad, A. Robert McCormack, B. François, A unified failure criterion for unstabilized rammed earth materials upon varying relative humidity conditions, Constr. Build. Mater. 95 (2015) 437–447. https://doi.org/10.1016/j.conbuildmat.2015.07.100.

6] B. François, L. Palazon, P. Gerard, Structural behaviour of unstabilized rammed earth constructions submitted to hygroscopic conditions, Constr. Build. Mater. 155 (2017) 164–175. https://doi.org/10.1016/j.conbuildmat.2017.08.012.

7] A. Fabbri, L. Soudani, F. McGregor, J. C. Morel, Analysis of the water absorption test to assess the intrinsic permeability of earthen materials, Constr. Build. Mater. 199 (2019) 154–162. https://doi.org/10.1016/j.conbuildmat.2018.12.014.

8] H. Janssen, A discussion of "Analysis of the water absorption test to assess the intrinsic permeability of earthen materials", Constr. Build. Mater. 215 (2019) 1044–1046. https://doi.org/10.1016/j.conbuildmat.2019.05.016.

9] J. Carmeliet, H. Hens, S. Roels, O. Adan, H. Brocken, R. Cerny, Z. Pavlik, C. Hall, K. Kumaran, L. Pel, Determination of the liquid water diffusivity from transient moisture transfer experiments, J. Therm. Envelope Build. Sci. 27 (2004) 277–305. https://doi.org/10.1177/1097196304042324.

10] S. Roels, J. Carmeliet, Analysis of moisture flow in porous materials using microfocus X-ray radiography, Int. J. Heat Mass Transf. 49 (2006) 4762–4772. https://doi.org/10.1016/j.ijheatmasstransfer.2006.06.035.

11] J. Crank, The Mathematics of Diffusion, Oxford University Press, Oxford, 1989.

12] P. Ren, C. Feng, H. Janssen, Hygric properties of porous building materials (V): Comparison of different methods to determine moisture diffusivity, Build. Environ. 164 (2019) 106344. https://doi.org/10.1016/j.buildenv.2019.106344.

13] M. Hall, Y. Djerbib, Moisture ingress in rammed earth: Part 1 - The effect of soil particle-size distribution on the rate of capillary suction, Constr. Build. Mater. 18 (2004) 269–280. https://doi.org/10.1016/j.conbuildmat.2003.11.002.

14] M. L. Indekeu, C. Feng, H. Janssen, M. Woloszyn, Experimental study on the capillary absorption characteristics of rammed earth, Constr. Build. Mater. 283 (2021) 122689. https://doi.org/10.1016/j.conbuildmat.2021.122689.

15] M. A. Wilson, W. D. Hoff, C. Hall, Water movement in porous building materials - XIII. Absorption into a two-layer composite, Build. Environ. 30 (1995) 209–219. https://doi.org/10.1016/0360-1323(94)00035-Q.

16] M. A. Wilson, W. D. Hoff, C. Hall, Water movement in porous building materials - XIV. Absorption into a two-layer composite ($S_A < S_B$), Build. Environ. 30 (1995) 221–227. https://doi.org/10.1016/0360-1323(94)00036-R.

17] H. Janssen, H. Derluyn, J. Carmeliet, Moisture transfer through mortar joints: A sharp-front analysis, Cem. Concr. Res. 42 (2012) 1105–1112.

18] C. Feng, H. Janssen, Hygric properties of porous building materials (III): Impact factors and data processing methods of the capillary absorption test, Build. Environ. 134 (2018) 21–34. https://doi.org/10.1016/j.buildenv.2018.02.038.

19] A. N. Narayanaswamy, Mechanical testing procedure for local building materials: rammed earth and laterite building stones, Ecole nationale des travaux publics de l'Etat (2016).

20] A. Arrigoni, A.C. Grillet, R. Pelosato, G. Dotelli, C.T.S. Beckett, M. Woloszyn, D. Ciancio, Reduction of rammed earth's hygroscopic performance under stabilisation: an experimental investigation, Build. Environ. 115 (2017) 358– 367, https://doi.org/10.1016/j.buildenv.2017.01.034.

21] R. El Nabouch, Mechanical behavior of rammed earth walls under pushover tests, Université Grenoble Alpes & Université Savoie Mont Blanc (2017).

22] C. Feng, H. Janssen, Y. Feng, Q. Meng, Hygric properties of porous building materials: Analysis of measurement repeatability and reproducibility, Build. Environ. 85 (2015) 160–172. https://doi.org/10.1016/j.buildenv.2014.11.036.

23] E. Vereecken, Hygrothermal analysis of interior insulation, KU Leuven (2013).

24] B. J. Pease, G. A. Scheffler, H. Janssen, Monitoring moisture movements in building materials using X-ray attenuation: Influence of beam-hardening of polychromatic X-ray photon beams, Constr. Build. Mater. 36 (2012) 419–429. https://doi.org/10.1016/j.conbuildmat.2012.04.126.

25] J. Carmeliet, T. van Besien, S. Roels, New indirect estimation technique for the determination of the moisture diffusivity from transient moisture content profiles measured by means of X-ray radiography, Proc. 2nd Int. Conf. Research in Building Physics (2003) 159–167.
26] P. Moonen, T. Wangler, An analytical approach to the characterization of swelling in clay-bearing stone, Phil. Mag. 95 (2015) 3103–3121. https://doi.org/10.1080/14786435.2015.1063788.
27] C. Evangelides, G. Arampatzis, A.-A. Tsambali, E. Tzanetaki, C. Tzimopoulos, Moisture estimation in building materials with a simple procedure, Constr. Build. Mater. 164 (2018) 830–836.
28] Delphin 6 [computer software]. Available online: http://bauklimatik-dresden.de/delphin (accessed 24 August 2021).
29] S. Vogelsang, H. Fechner, A. Nicolai, Delphin 6 Material File Specification, Version 6.0, Technical Report.